TECHNICAL REPORT No. 19

(12)

TO

THE OFFICE OF NAVAL RESEARCH
CONTRACT No. N00014-76-C-0037, NR 031-756

DEFORMATION AND FRACTURE OF STRONGLY TEXTURED Ti ALLOY SHEET IN UNIAXIAL TENSION

K. S. CHAN* AND D. A. KOSS

DEPARTMENT OF METALLURGICAL ENGINEERING
MICHIGAN TECHNOLOGICAL UNIVERSITY
HOUGHTON, MICHIGAN U.S.A.

*CURRENTLY: DEPARTMENT OF MATERIALS SCIENCE
AND ENGINEERING
STANFORD UNIVERSITY
STANFORD, CA

SECURITY CLASSIFICATION OF THIS PAGE (When Data Entered)

REPORT DOCUMENTATION PAGE		READ INSTRUCTIONS BEFORE COMPLETING FORM
1. REPORT NUMBER No. 19	2. GOVT ACCESSION NO. AD-A115409	3. RECIPIENT'S CATALOG NUMBER
4. TITLE (and Subtitle) Deformation and Fracture of Strongly Textured Ti Alloy Sheet in Uniaxial Tension		5. TYPE OF REPORT & PERIOD COVERED 6. PERFORMING ORG. REPORT NUMBER
7. AUTHOR(s) K. S. Chan and D. A. Koss		8. CONTRACT OR GRANT NUMBER(s) N00014-76-C-0037 NR 031-756
9. PERFORMING ORGANIZATION NAME AND ADDRESS Department of Metallurgical Engineering Michigan Technological University Houghton, Michigan 49931		10. PROGRAM ELEMENT, PROJECT, TASK AREA & WORK UNIT NUMBERS
11. CONTROLLING OFFICE NAME AND ADDRESS Office of Naval Research 800 N. Quincy Street Arlington, VA 22217		12. REPORT DATE April, 1982 13. NUMBER OF PAGES 30
14. MONITORING AGENCY NAME & ADDRESS(if different from Controlling Office)		15. SECURITY CLASS. (of this report) Unclassified 15a. DECLASSIFICATION/DOWNGRADING SCHEDULE

16. DISTRIBUTION STATEMENT (of this Report)

Distribution of this document is unlimited.

17. DISTRIBUTION STATEMENT (of the abstract entered in Block 20, if different from Report)

18. SUPPLEMENTARY NOTES

19. KEY WORDS (Continue on reverse side if necessary and identify by block number)

Deformation, fracture, uniaxial tension, Ti-6Al-4V, Ti-5Al-2.5SN, plastic anisotropy

20. ABSTRACT (Continue on reverse side if necessary and identify by block number)

The influence of crystallographic texture on the deformation and fracture behavior of strongly textured Ti alloy sheet has been investigated. Uniaxial tensile tests have been performed on Ti-6Al-4V and Ti-5Al-2.5Sn sheet with either a basal or basal-transverse texture. The results indicate that, by controlling the ease of through-thickness slip, the crystallographic texture strongly affects the plastic anisotropy of the material but has relatively little effect on the work-hardening rate and strain-rate sensitivity. (Cont'd)

DD FORM 1 JAN 73 1473 EDITION OF 1 NOV 65 IS OBSOLETE
S/N 0102-014-6601

SECURITY CLASSIFICATION OF THIS PAGE (When Data Entered)

20. Abstract (cont'd)

A strong resistance to through-thickness slip, manifested by a high R-value, enhances the post-uniform elongation and the ability of the material to retain the load carrying capacity beyond maximum load. This behavior can be qualitatively understood in terms of the effect of R on the hardening which occurs as the strain state within the diffuse neck shifts from uniaxial tension toward plane strain. A higher R-value also increases significantly the limit strain at the onset of localized necking as well as the fracture strain. The effects of R-value on the limit strain can be qualitatively understood in terms of a critical thickness strain criterion. Calculations of limit strains using an inclined imperfection model are also in good agreement with experimental results.

Deformation and Fracture of Strongly Textured Ti Alloy Sheet in Uniaxial Tension

By

K. S. Chan[+] and D. A. Koss
Department of Metallurgical Engineering
Michigan Technological University
Houghton, Michigan 49931

Abstract

The influence of crystallographic texture on the deformation and fracture behavior of strongly textured Ti alloy sheet has been investigated. Uniaxial tensile tests have been performed on Ti-6Al-4V and Ti-5Al-2.5 Sn sheet with either a basal or basal-transverse texture. The results indicate that, by controlling the ease of through-thickness slip, the crystallographic texture strongly affects the plastic anisotropy of the material but has relatively little effect on the work-hardening rate and strain-rate sensitivity. A strong resistance to through-thickness slip, manifested by a high R-value, enhances the post-uniform elongation and the ability of the material to retain the load carrying capacity beyond maximum load. This behavior can be qualitatively understood in terms of the effect of R on the hardening which occurs as the strain state within the diffuse neck shifts from uniaxial tension toward plane strain. A higher R-value also increases significantly the limit strain at the onset of localized necking as well as the fracture strain. The effects of R-value on the limit strain can be qualitatively understood in terms of critical thickness strain criterion. Calculations of limit strains using an inclined imperfection model are also in good agreement with experimental results.

+Currently: Department of Materials Science and Engineering,
Stanford University, Stanford, CA 94305

INTRODUCTION

Titanium alloys in sheet form usually possess crystallographic textures which, in some instances, can be quite strong.[1-4] Due to the nature of slip in the hcp α-phase, strong textures in α-β Ti alloys often exert a pronounced influence on mechanical properties. Many of these effects are well documented for an alloy such as Ti-6Al-4V in the form of plate and bar stock.[1,4-7] In the case of sheet metal deformation, a crystallographic texture usually results in plastic anisotropy, the degree of which is measured by the parameter R which is the ratio of the width strain to thickness strain in a uniaxial tensile test. Previous studies of the deformation of strongly textured Ti alloy sheet have been primarily confined to multiaxial yielding behavior and texture strengthening as influenced by the very wide range of R-values (0.2-14) possible in these alloys.[1-3,8-11] Large strain deformation of Ti and Ti-6Al-4V sheet has been previously examined in order to determine the effect of strain hardening and strain rate hardening on necking behavior in uniaxial tension [12] and forming limit strains in stretch forming behavior.[13,14] However, the R-value was not varied in these studies, and no attempt has been made to determine the influence of R on large strain deformation of Ti and its alloys.

Large strain deformation and the phenomenon of localized necking in sheet metal has been studied in considerable detail in steel, brass, and aluminum alloys (see, for example, ref. 15,16). It is well established in these materials that strain hardening and strain rate hardening are both important in enhancing the resistance to localized necking and thus the formability. The influence of crystallographic texture and R-value on the stretch formability is, however, less conclusive.[15,17-19] The experimental difficulty has been in manipulating sheet metal processing to vary R over a large range of values without changing other properties such as strain hardening exponent, n, and

the strain rate sensitivity exponent, m. In addition, owing to the nature of slip in fcc and bcc metals, the range of R-values studied is not large; usually $0.5 \leq R \leq 2$. It is therefore difficult to separate the effect of crystallographic texture and R value from that of n and m. Thus our knowledge of the influence of plastic anisotropy on the large strain deformation of sheet material is limited by the nature of the experimental studies to date.

This investigation examines the influence of crystallographic texture on the post-uniform deformation and the process of localized necking and fracture behavior of strongly textured Ti-6Al-4V (Ti-6-4) and Ti-5Al-2.5 Sn (Ti-5-2.5) sheet tested in uniaxial tension. Photo-gridded specimens are used throughout so that detailed strain measurements can be made in order to determine the effect of the R-value on the development of localized necking as well as on the magnitudes of the forming limit and fracture strains. Manipulating the crystallographic texture of the Ti-alloy sheet to yield a wide range of R-values but with relatively constant n and m values, the influence of the R-value on the strain localization process can be separated from that due to strain hardening and strain rate sensitivity (i.e., n and m). The present study examines the behavior in uniaxial tension; the behavior of strongly textured Ti-6-4 and Ti-5-2.5 sheet under multiaxial deformation conditions, utilizing punch-stretch testing [19], is reported separately.[21]

EXPERIMENTAL

Thin sheet specimens (1.4mm thick) of Ti-6Al-4V and Ti-5Al-2.5 Sn with strong crystallographic texture were prepared by hot rolling. In processing the Ti-6-4 and Ti-5-2.5 sheet with the basal texture, 2.5cm thick blocks were 90° cross rolled at 816°C [2,3] to a final sheet thickness of 1.4mm. Reheating the sheet between each pass was necessary; the thickness reduction of each pass was initially 2.5mm and was gradually decreased to 0.25mm at the final

stage of the rolling process. Ti-6-4 sheet with the basal-transverse texture was processed from 6.4mm thick plate kindly supplied by Del West Associates; the plate material already possessed a basal-transverse texture obtained by the thermal cascade rolling method developed by Sommer and Creager.[4] For the present study, the plate was hot rolled at 734°C, reheating after each pass, until sheet with a thickness of 1.4mm was attained. After hot rolling, all of the sheet material was descaled by sand blasting and then pickled with a warm acid solution of 5% HF, 35% HNO_3, and 60% H_2O at 150°C for 30-45 minutes. This pickling procedure removed the oxides and provided clean, smooth surfaces for both Ti-6-4 as well as Ti-5-2.5 sheet. No local attack on the surface of the sheet was observed. Finally, after machining, the specimens were heat treated at 734°C at a pressure of $<2.7 \times 10^{-4}$ Pa for four hours and quenched. The chemical compositions of the Ti-6-4 and Ti-5-2.5 sheet specimens (after heat treatment), are shown in Table I.

Fig. 1 shows the equiaxed α-β microstructure for both the basal-transverse (Fig. 1a) and the basal (Fig. 1b) textured Ti-6-4 specimens. The volume fraction of the β phase is about 24% while the grain size is approximately 10μ for both cases. The microstructure of the basal-textured Ti-5-2.5 alloy is primarily α-phase with a grain size of 14 and a small amount of retained β-phase.

The texture of Ti-6-4 and Ti-5-2.5 sheets were determined by x-ray diffraction method performed by Boeing Technology Services, Seattle, Washington. Pole figures for basal textured Ti-6-4 and Ti-5-2.5 and basal-transverse textured Ti-6-4 are shown in Fig. 2a, b, and c respectively. The strong alignment of the basal plane poles should be noted.

Tensile specimens were machined to a 50.8mm gauge length and 19mm in width. Uniaxial tensile testing was performed at room temperature at a constant crosshead speed at an initial strain rate of 8.3×10^{-5} s^{-1}. Local

Table I. The chemical compositions of the textured Ti-6Al-4V and Ti-5Al-2.5Sn sheet.

Material	Texture	Composition, Wt. Pct. Al	V	Sn	C	H	O	N
Ti-6Al-4V	Basal	5.83	3.92	-	0.014	0.0014	0.120	0.013
Ti-6Al-4V	Basal-transverse	6.06	3.76	-	0.020	0.0008	0.172	0.017
Ti-5Al-2.5Sn	Basal	5.23	-	2.43	0.018	0.0007	0.135	0.015

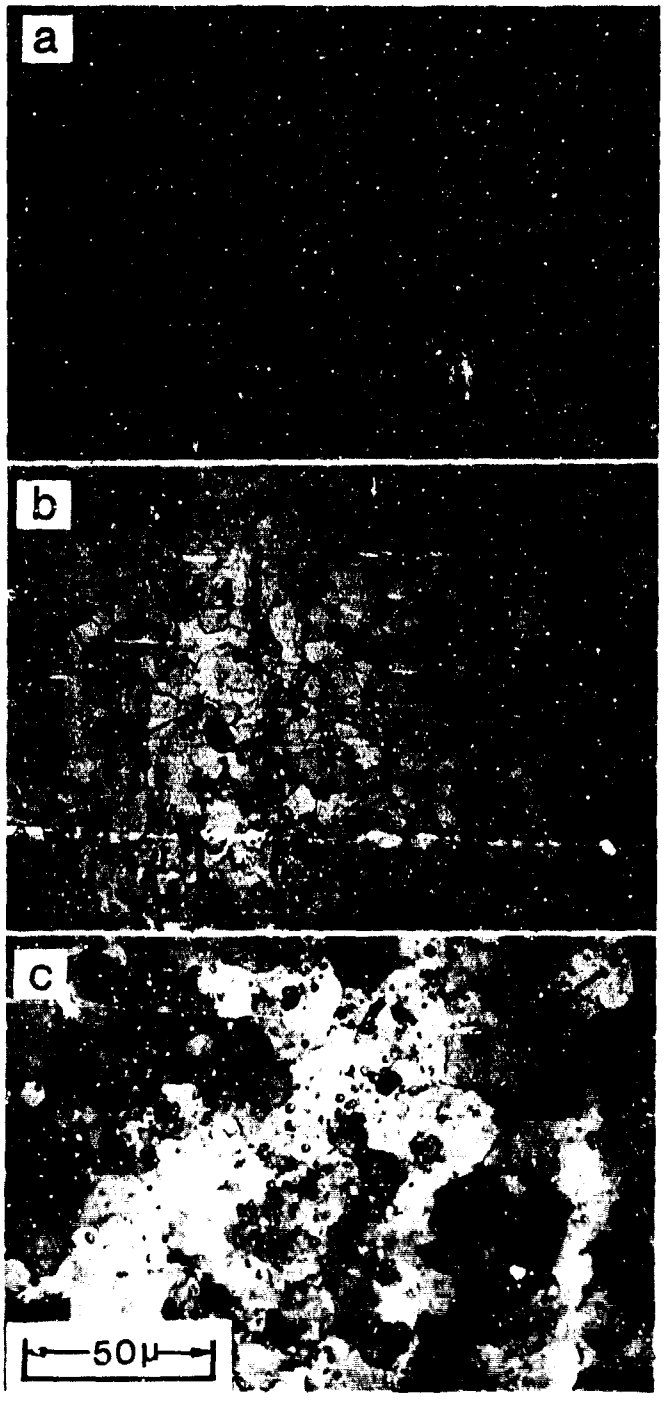

Fig. 1. Optical micrographs showing the microstructures in the plane of the sheet of: (a) basal textured Ti-6Aℓ-4V, (b) basal-transverse textured Ti-6Aℓ-4V, and (c) basal textured Ti-5Aℓ-2.5Sn.

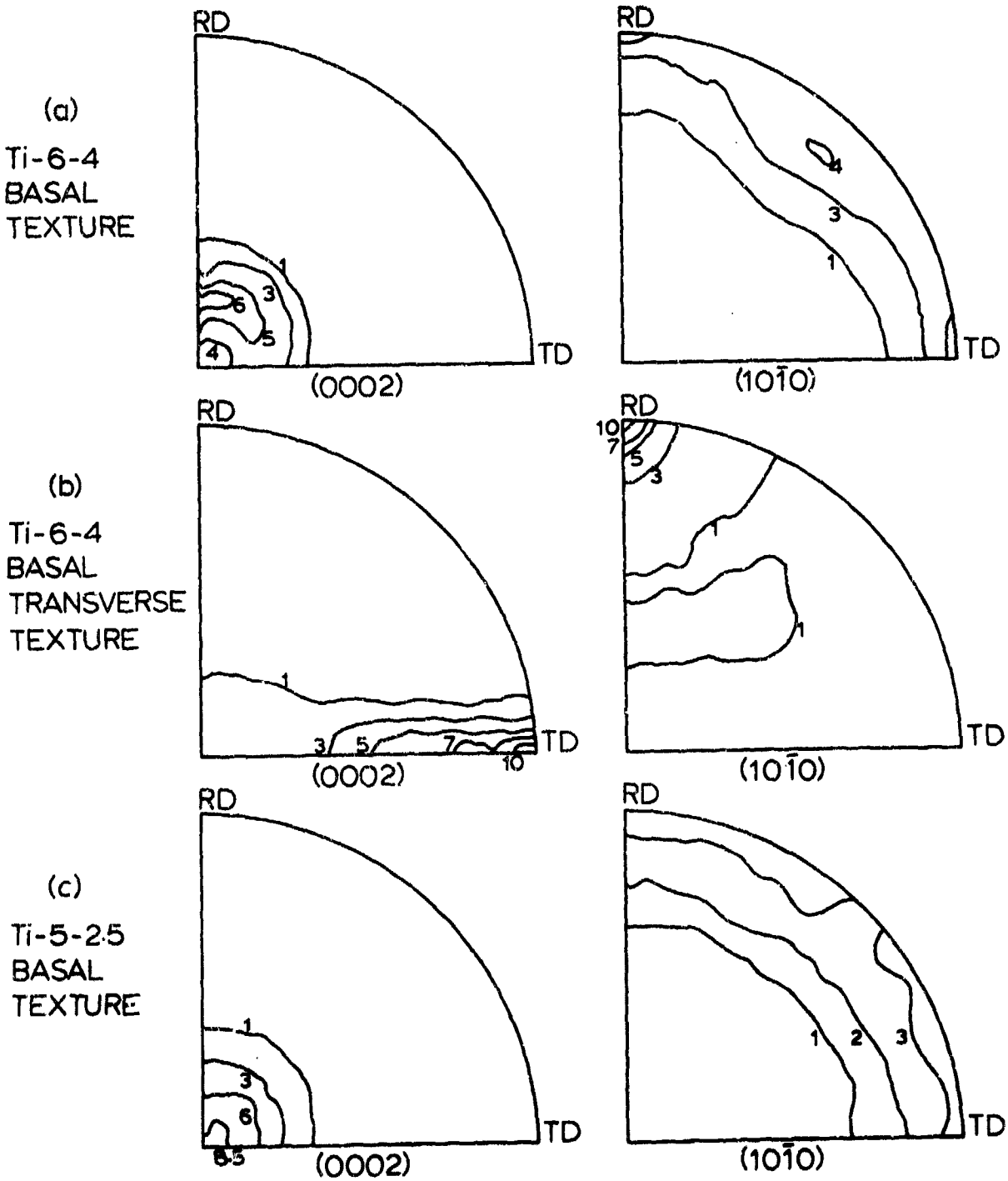

Fig. 2. Pole figures showing the crystallographic textures of: (a) basal textured Ti-6Al-4V sheet, (b) basal-transverse textured Ti-6Al-4V sheet, and (c) basal textured Ti-5Al-2.5Sn.

strains were obtained from measurements of the deformed photogrids using a measuring microscope. The R-value has been obtained from strain measurements of the deformed photogrids on the tensile specimens at selected stages of deformation prior to diffuse necking.

RESULTS

Fig. 3 shows the stress-strain behavior of textured Ti-6-4 and Ti-5-2.5 sheet. The yield stress and the work hardening behavior of the basal textured Ti-6-4 and Ti-5-2.5 sheet (Fig. 3a) are independent of the orientation of the stress axis. In contrast, the basal-transverse textured Ti-6-4 sheet manifests planar anisotropy; both the .2% offset yield stress and the work hardening rate vary with the orientation of the stress axis as seen in Fig. 3b. The effects of crystallographic texture on the tensile yield stress, the work hardening exponent ($n = \frac{d\ln\sigma}{d\ln\varepsilon}$), strain-rate sensitivity ($m = \frac{d\ln\sigma}{d\ln\dot{\varepsilon}}$), and plastic anisotropy parameter (R) are summarized in Fig. 4. An especially noteworthy result is that the influence of crystallographic texture on the work hardening exponent (n) and the strain rate sensitivity (m) is small when compared to the large changes in the plastic anisotropy parameter, R. The n and m values of the textured Ti-6-4 and Ti-5-2.5 sheet are relatively constant ($n \approx 0.040$-0.066, $m = 0.012$-0.016), while the R- value changes from 0.5 to 12. It should also be noted that the uniaxial yield stress of the basal-transverse Ti-6-4 depends strongly on specimen orientation with the TD (or near-TD) specimens having $\sim$25% higher yield stress than those tested parallel to or near the RD.

Typical strain distributions along the gauge length of a tensile specimen at different stages of deformation are shown in Fig. 5. The effect of the R-value on the axial strain distribution is shown in Fig. 6. As may be seen in Fig. 6, increasing R-value not only increases the limit strains (denoted by the arrows) at the onset of localized necking but also increases the breadth of the diffuse neck.

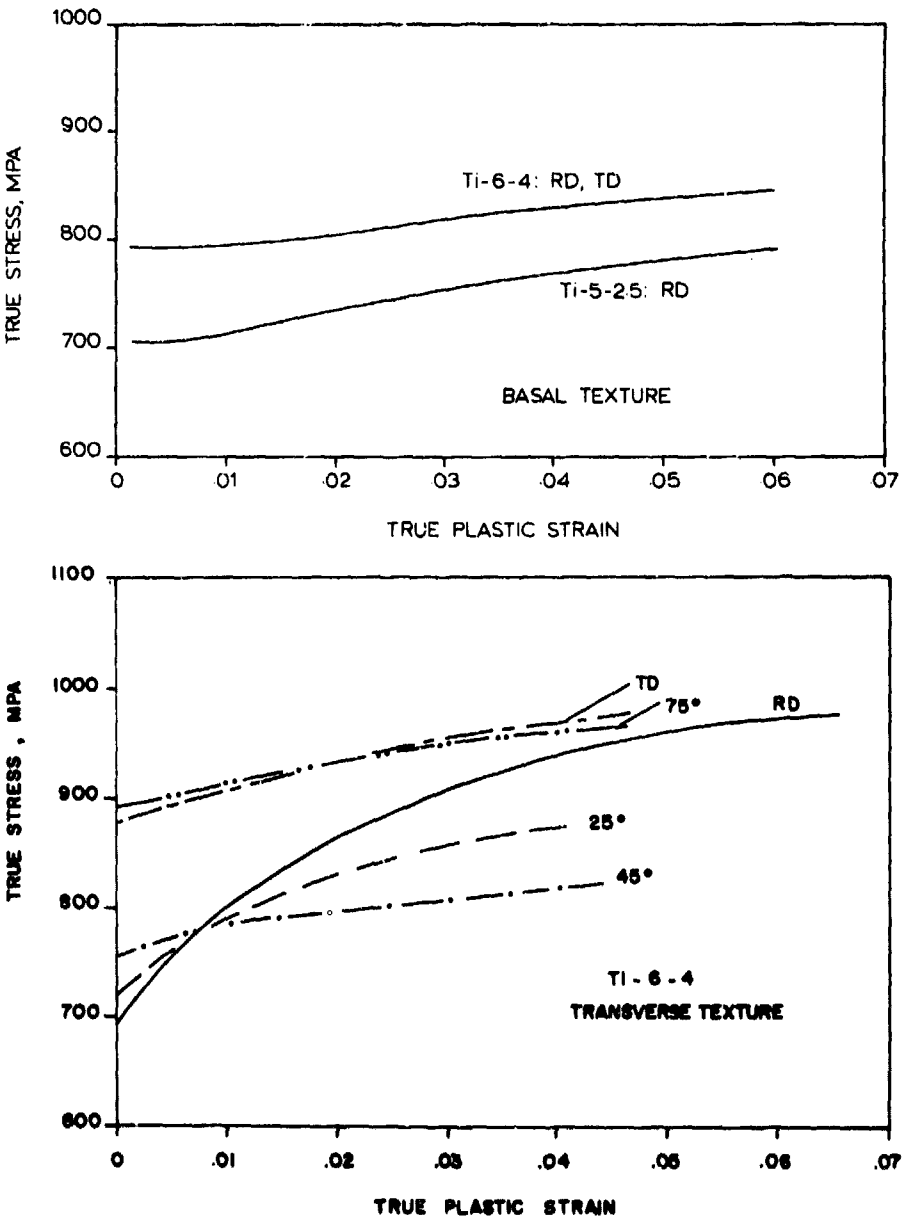

Fig. 3. True stress-true strain curves for: (a) basal textured Ti-6-4 and Ti-5-2.5 and (b) basal-transverse textured Ti-6-4 as a function of the orientation of the tensile axis. TD denotes that the tensile axis is parallel to the transverse direction, while RD is parallel to the rolling direction. The angles indicate inclination to the RD.

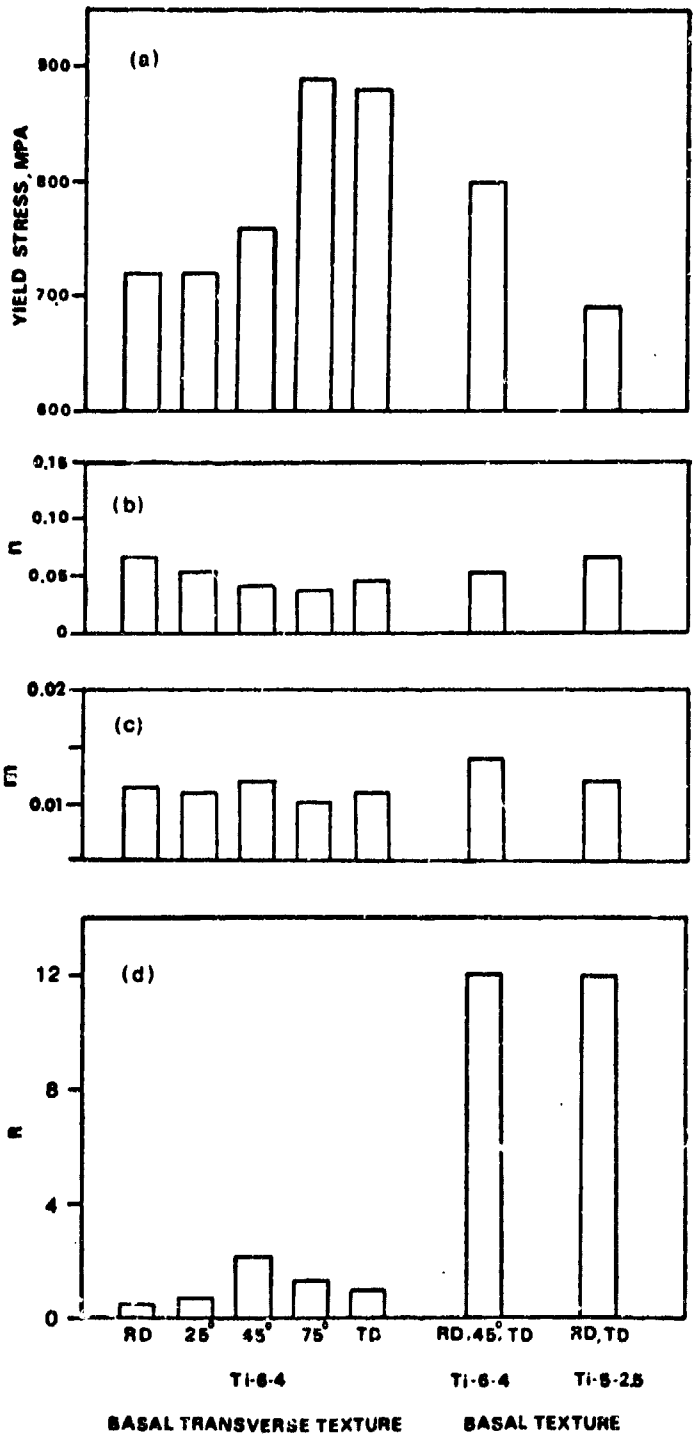

Fig. 4. The effects of crystallographic texture and orientation of the tensile axis on the behavior of Ti-6-4 and Ti-5-2.5 sheet for the: (a) yield stress, (b) work hardening exponent n, (c) strain hardening exponent m, and (d) plastic anisotropy parameter R.

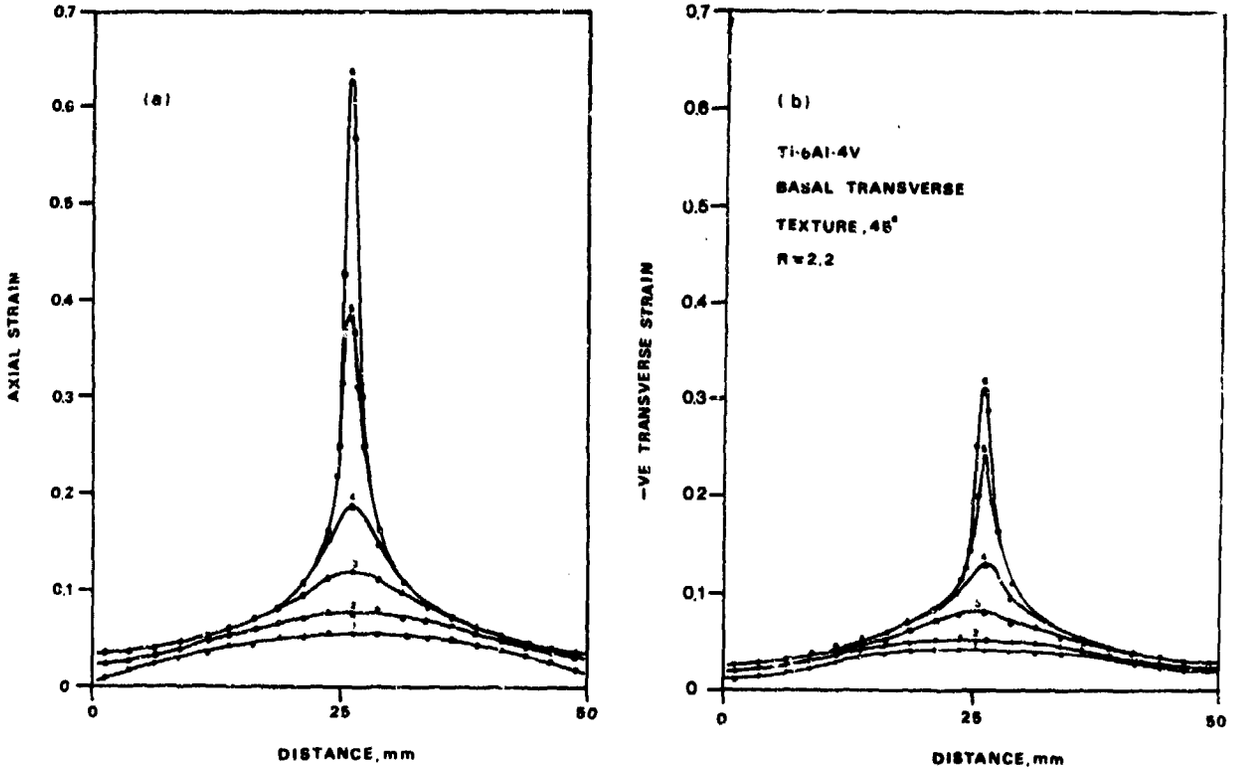

Fig. 5. The strain distribution along the 5 cm gauge length of a tensile specimen at four stages of deformation of a basal textured Ti-6-4 specimen.

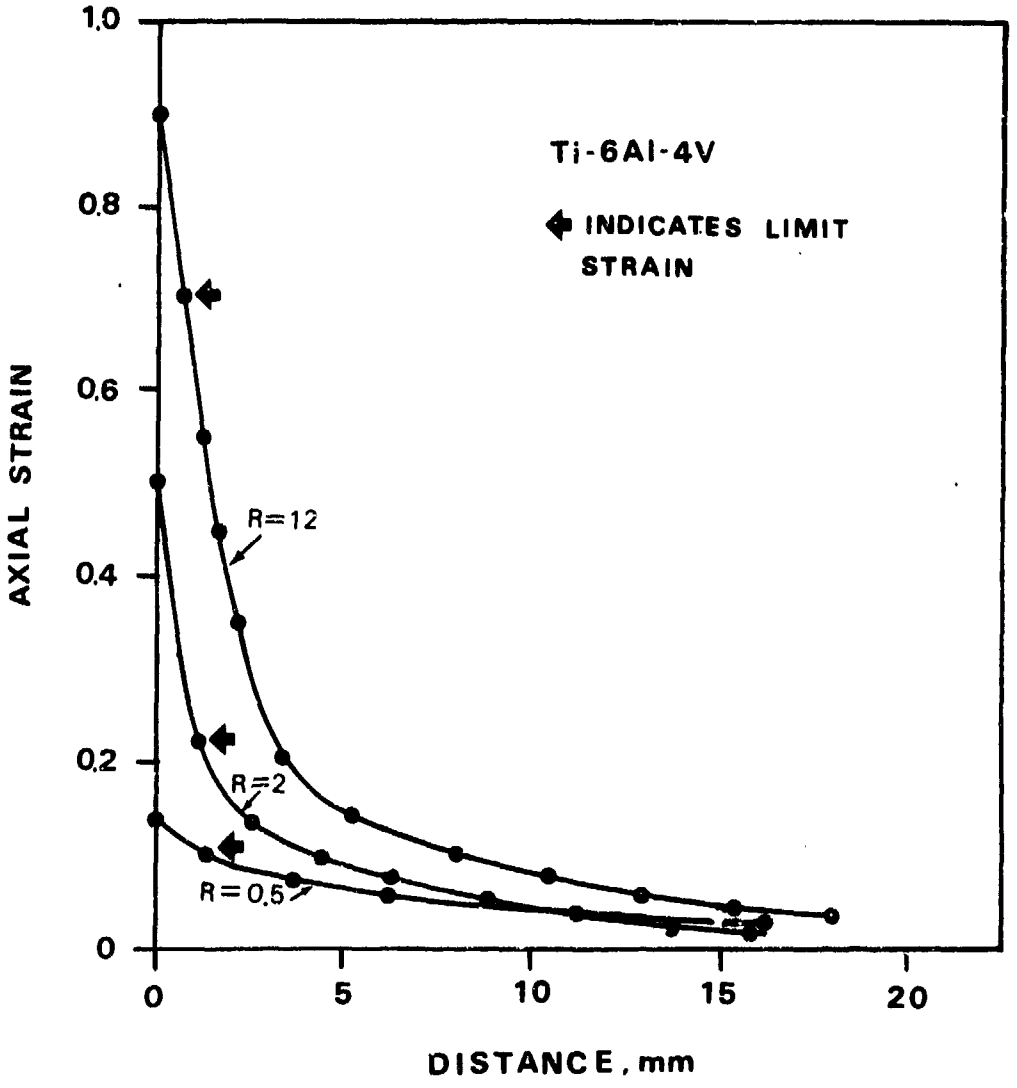

Fig. 6. The distribution of the axial strain with position along the gauge length for Ti-6-4 sheet specimens with differing textures and R-values. The limit strain for the onset of localized necking is indicated.

Tracing the strain histories of several grid elements, the dependence of the negative transverse strain $-\varepsilon_y$ on the axial strain ε_x may be determined. As depicted in Fig. 7, a linear relationship occurs between $-\varepsilon_y$ and ε_x at strains which are greater than the strain at maximum load but less than the forming limit strain*. The slope of the linear region defines the strain ratio $\rho = \frac{d\varepsilon_y}{d\varepsilon_x}$, which also equals -R/(1+R) for uniaxial tension. Fig. 7 indicates that the plane strain condition ($\rho = \frac{d\varepsilon_y}{d\varepsilon_x} = 0$) is easily attained at low strain levels when R = 0.5. As the R-value increases to 2.2 and especially to 12, the plane strain condition becomes increasingly difficult to achieve and occurs at larger strains.

Beginning with the maximum load P_{max} on the load P vs. extension δ chart, Fig. 8 shows the normalized load P/P_{max} as a function of the extension δ as a means of depicting the loss of load carrying ability due to diffuse necking. As indicated in Fig. 8, basal textured Ti-6-4 and Ti-5-2.5 sheet shown an identical rate of load loss which, in turn, is much more gradual than that of the basal-transverse textured Ti-6-4. In the basal textured Ti-6-4 sheet, the load carrying capacity is retained best when the loading direction is 45° from the rolling direction and the R-value is 2.2. RD and TD specimens (R is 0.5 and 1.0, respectively), on the other hand, show a rapid loss of load carrying ability. Comparing the mechanical properties of the material, the results in Fig. 8 clearly indicate that a large R value is beneficial in retaining load carrying capacity beyond diffuse necking. At low R values ($R \leq 1$), the trend is not so obvious; other parameters such as n and m may also be important.

The onset of diffuse necking of a sheet tensile specimen is characterized by a gradual development of a neck with a profile radius that decreases from

---

* ε_x and ε_y are also the principal strains; therefore, $\varepsilon_x = \varepsilon_1$ and $\varepsilon_y = \varepsilon_2$, except for the 25°, 45° and 75° cases in the basal-transverse textured material.

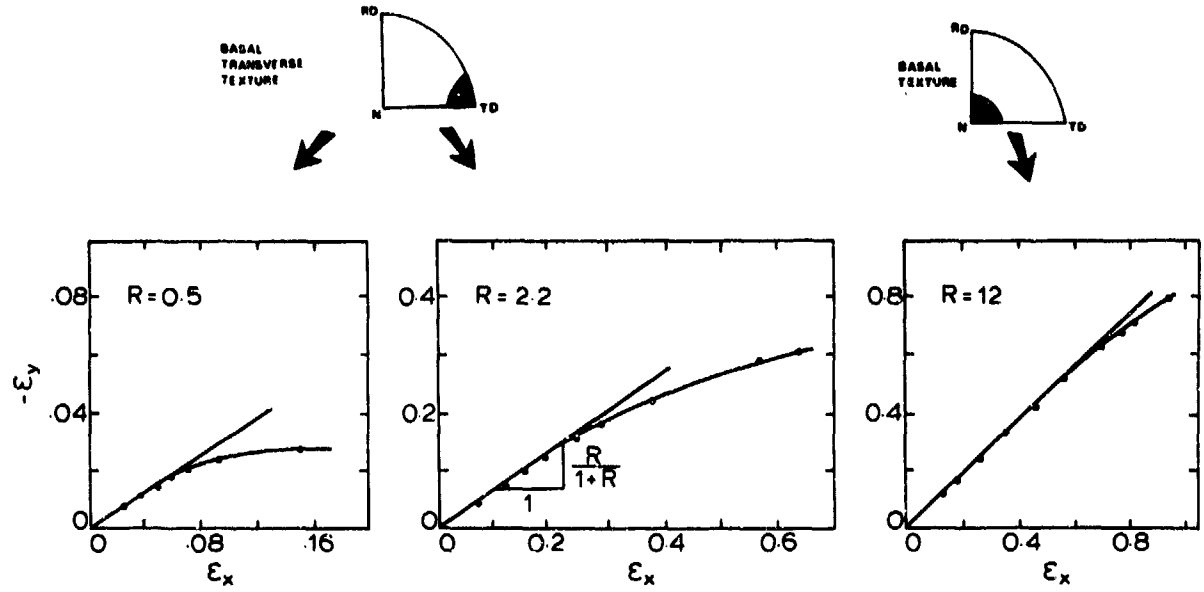

Fig. 7. The dependence of the transverse strain ε_y on the axial strain ε_x during uniaxial tensile deformation of Ti-6Al-4V sheet with R-values of 0.5, 2.2, and 12. Note the differences in scales.

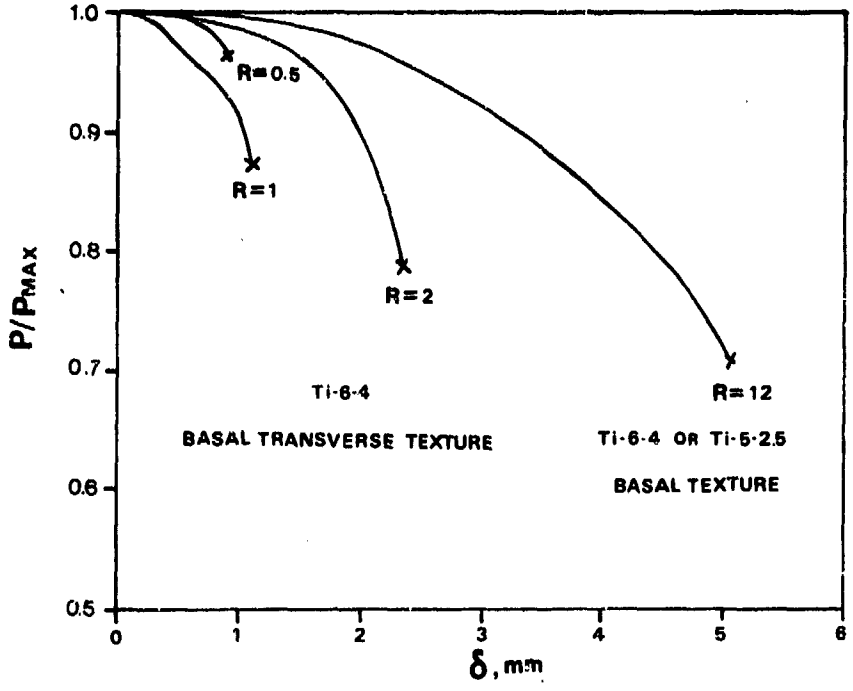

Fig. 8. The post-uniform load-carrying capacity, as measured by instantaneous load P normalized with respect to maximum load P_{max}, as a function of extension δ for Ti-6-4 and Ti-5-2.5 sheet with different R-values.

infinity to some finite value as straining continues. The influence of crystallographic texture and thus R-value on the tensile neck profile is illustrated in Fig. 9. For the Ti-6-4 sheet with the basal-transverse texture as tested in the RD (R = 0.5), the diffuse neck is very small and is characterized by a very small reduction in the width of the specimen and thus a large neck profile radius (see Fig. 9, R = 0.5). The diffuse neck is still gradual but is quite apparent when R = 2 for Ti-6-4 sheet with the basal-transverse texture but stressed at 45° to the RD. A much more sharp diffuse neck profile is observed in the basal textured Ti-6-4 sheet with R = 12.

The influence of texture on the tensile strain to fracture ε_{1f} is indicated in Fig. 10 together with the associated fractographs. The detailed dependence of the fracture strain ε_{1f} on the R-value is complicated although the values reported in Fig. 10 indicate that the fracture strain increases with the R-value. Fractography, also shown in Fig. 10, indicates that fracture of textured Ti-6-4 and Ti-5-2.5 sheet occurs by ductile fracture with the fracture surface characterized by dimples. Small, shallow dimples indicating low ductility are observed for the basal-transverse texture sheet with a low R-value (R = 0.5) and the smallest fracture strain (ε_{1f} = 0.17). On the other hand, the dimples are significantly larger and deeper in the material with the highest fracture strain (ε_{1f} = 0.93) and the R-value (R = 12).

DISCUSSION

Effects of Crystallography on Plastic Anisotropy

The basal textured Ti-6-4 and Ti-5-2.5 sheet exhibits a strong tendency for the basal plane of the hcp α- phase to lie in the plane of the sheet; see Figs. 2a and 2c. Thus, the <11$\bar{2}$0> slip directions for basal (001), prism {10$\bar{1}$0} and pyramidal {10$\bar{1}$1} slip will also be contained in the plane of the

*The fracture strain ε_{1f} is calculated from the equation: $\varepsilon_{1f} = -\varepsilon_{2f} - \varepsilon_{3f}$ where ε_{3f} and ε_{2f} are respectively the thickness strain and the transverse strain of deformed grids located near the fracture surface.

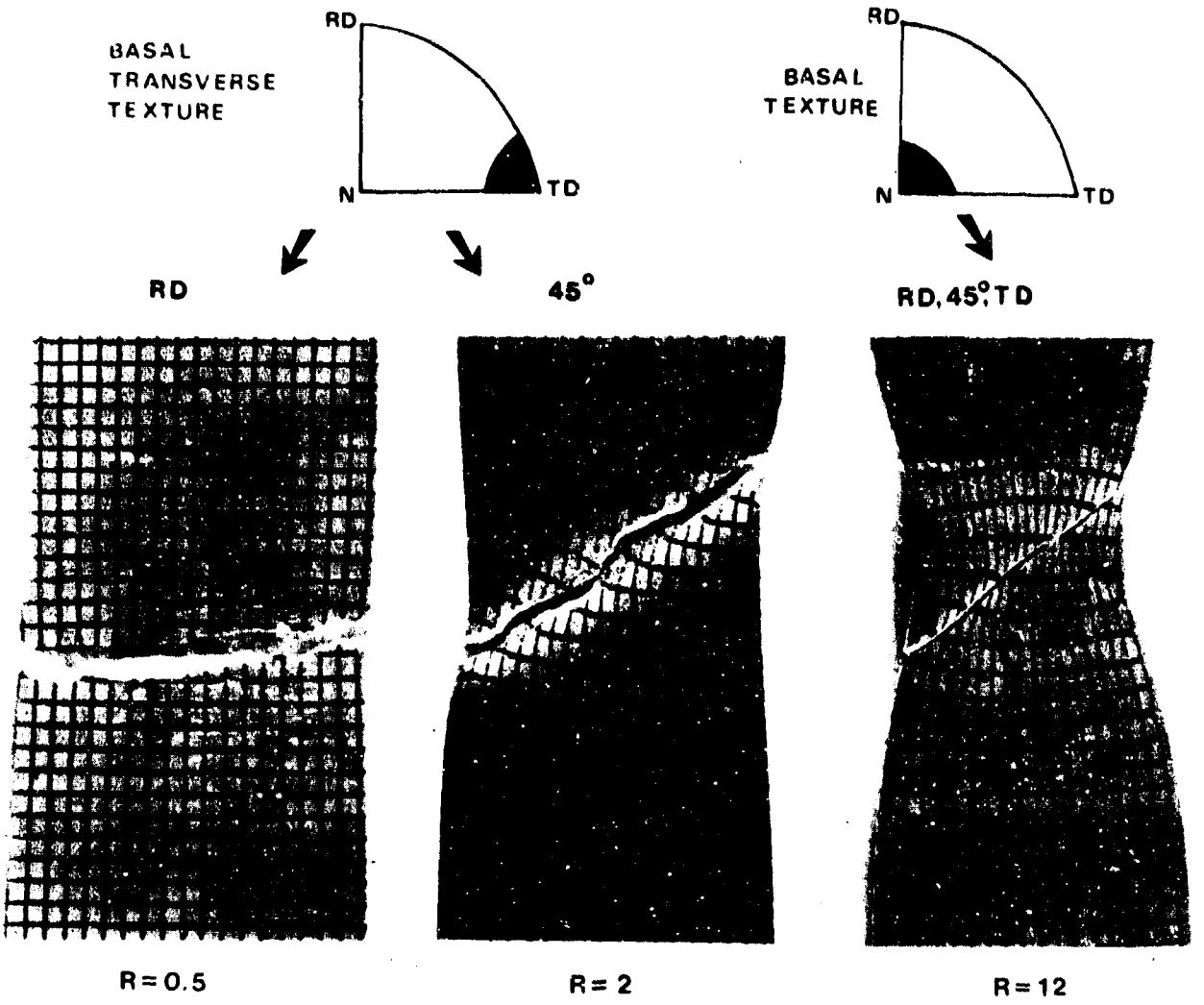

Fig. 9. The influence of the crystallographic texture and R-value on the profile of the diffuse neck and the orientation of the localized neck (as indicated by the fracture). The material is Ti-6Al-4V sheet.

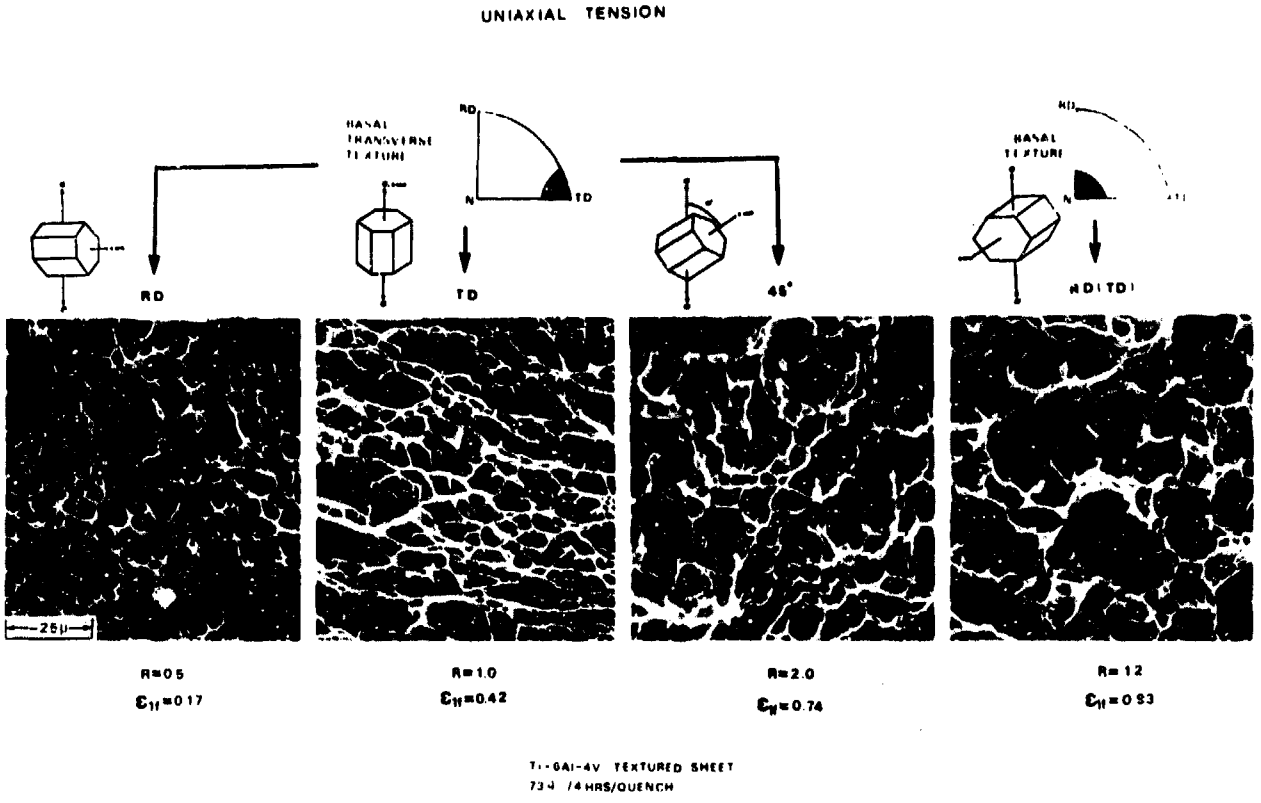

Fig. 10. Scanning electron micrographs showing the fracture surfaces of Ti-6-4 sheet specimens with R-values ranging from 0.5-12. Note the corresponding values for the major principal strain at fracture ε_{1f}, measured locally across the fracture surface.

sheet for a large fraction of the grains present. Through-thickness deformation of the basal textured sheet is therefore difficult as it would require twinning or the activation of $\vec{c} + \vec{a}$ slip. Width contraction, on the other hand, can occur readily by prism slip and thus longitudinal tensile extension can be accommodated primarily by width contraction. The result is a high R-value (R = 12) exhibited by basal textured sheet. The absence of an alignment of the prism planes in the material with a basal texture (see Figs. 2a and 2c) also results in stress-strain behavior which is similar in the RD, TD and the 45° direction. The yield stress, work hardening exponent ($n \simeq 0.05$), strain rate sensitivity ($m \simeq 0.014$) and the plastic anisotropy parameter (R = 12) are all approximately independent of the orientation of the stress axis. The basal textured sheet specimens of Ti-6-4 and Ti-5-2.5 thus exhibit "normal anisotropy" as they are isotropic on the plane of the sheet but anisotropic in the thickness direction.

In contrast, the basal-transverse Ti-6-4 sheet possesses a strong texture in which the (0002) and $\{10\bar{1}0\}$ poles tend to be aligned in the transverse and rolling direction, respectively (see Fig. 2b). Such a crystallographic orientation strongly favors through-thickness deformation by prism slip when tensile loading is applied in the rolling direction RD. However, activation of $\vec{a}$ slip becomes progressively more difficult as the stress axis is rotated toward the $\vec{c}$ axis in the transverse direction TD. Consequently, the basal-transverse textured Ti-6-4 sheet exhibits yield strengths which increase markedly from RD to TD. In addition, the R-value is also strongly dependent on the orientation of the stress axis in sheet with a basal-transverse texture. The lowest R-value of 0.5 occurs when the prism planes are oriented for easy through-thickness deformation as in the RD tests. The R-value increases to a value of 2.2 when stressed at 45° from the rolling direction. The basal-transverse textured Ti-6-4 sheet is thus anisotropic in the plane of the sheet (planar

anisotropy). On the other hand the strain rate sensitivity and the strain hardening exponents are relatively constant ($m \simeq 0.012$ and $n \simeq 0.05$) and independent of the orientation of the stress axis.

Plastic Instability and Fracture

The dependence of plastic instability and fracture on crystallographic texture is indicated by the influence of the R-value on the post-uniform elongation, the limit strain, the normalized fracture load, and the fracture strain; these effects are summarized in Fig. 11. Fig. 11a shows that a high R-value is beneficial in enhancing the post-uniform elongation e_{pu} (Fig. 11a) and the major principal limit strain ε_1^* (Fig. 11b) and in retaining the load carrying capacity (P/P_{max} in Fig. 11d) by increasing the fracture strain ε_{1f} (Fig. 11c). The $-\varepsilon_y$ vs. ε_x plot (recall $\varepsilon_x = \varepsilon_1$ and $\varepsilon_y = \varepsilon_2$) in Fig. 7 illustrates the beneficial effect of a high R-value in resisting localized necking by delaying the attainment of a plane strain condition ($\rho = d\varepsilon_y/d\varepsilon_x = 0$) within the diffuse neck. In contrast, as shown in Fig. 11a, the R-value has little effect on the uniform strain ε_u, the magnitude of which depends mainly on the work hardening exponent n, which is consistent with the Considere condition for diffuse necking. Finally, it is important to note in Fig. 11b that the thickness strain ($\varepsilon_3^* = (-\varepsilon_1^* - \varepsilon_2^*)$) at which localized necking occurs is approximately constant; thus ε_3 is observed to be <u>independent</u> of R-value.

Several of the effects in Fig. 11 can be viewed in terms of a "flow stabilizing influence" of a high R-value. Consider the mechanical equation of state for the axial stress σ_1 necessary to deform a tensile sheet specimen beyond uniform strain at temperature T to be represented by:

$$\sigma_1 = \sigma_1(\varepsilon, \dot{\varepsilon}, \rho, T), \tag{1}$$

where the strain ratio $\rho = \varepsilon_2/\varepsilon_1$ depends on strain and location within a diffuse neck. Plastic deformation within a diffuse neck is characterized by an

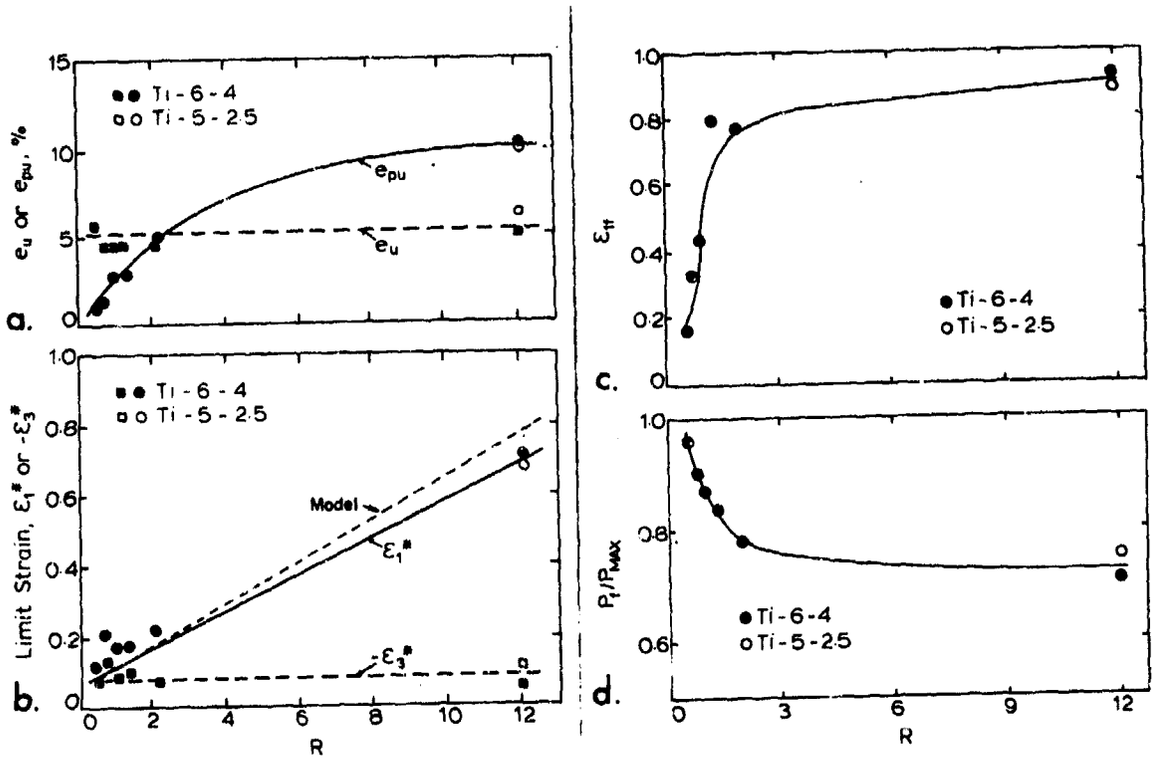

Fig. 11. The influence of R-value on: (a) the uniform strain e_u and post-uniform strain e_{pu}, (b) the major principal limit strain ε_1^* (both experimental and predicted) and minor (thickness) strain $-\varepsilon_3^*$, (c) the major principal strain at fracture ε_{1f}, and (d) the normalized fracture load P_f/P_{max}.

increase in strain rate and, as shown in Fig. 7, a change of strain state from uniaxial tension toward that of plane strain at the center of the neck. The condition for temporary restoration of plastic flow stability within the diffuse neck has been examined by Ghosh, [22] and for uniaxial tension it is:

$$\frac{1}{\sigma_1}\frac{\partial\sigma_1}{\partial\varepsilon}\frac{d\dot{\varepsilon}}{d\varepsilon}+\frac{1}{\sigma_1}\frac{\partial\sigma_1}{\partial\rho}\frac{d\rho}{d\varepsilon}+\frac{1}{\sigma_1}\frac{\partial\sigma_1}{\partial T}\frac{dT}{\partial\varepsilon}\geq 1-\frac{1}{\sigma_1}\frac{\partial\sigma_1}{\partial\varepsilon} \qquad (2)$$

The $\frac{\partial\sigma_1}{\partial\dot{\varepsilon}}$ and $\frac{\partial\sigma_1}{\partial\rho}$ terms in Eq. (2) represent contributions to neck stability due to axial stress increases arising from increased strain rate and a change in strain state respectively. It is well recognized that strain hardening and especially strain rate hardening are very beneficial in stabilizing plastic flow within the diffuse neck and in post-uniform elongation. However, the beneficial effect of "strain path" hardening due to the change in the strain state toward plane strain can also have a significant stabilizing influence; see for example, the discussion by Ghosh.[22] As can be readily visualized from the shape of the yield surface, the magnitude of the strain-path hardening effect increases with increasing R in a uniaxial tension test.[22] Thus a large R-value stabilizes plastic deformation within the diffuse neck as the material approaches plane strain at the center of the neck. Since the n and m-values of the sheet specimens in the present study are relatively constant, the flow stabilizing influence of a high R-value is primarily responsible for: (a) the difficulty in obtaining the plane strain condition $(d\varepsilon_y/d\varepsilon_x) = 0$ at high R-values in Fig. 7, (b) a more gradual loss of post-uniform load carrying capacity at high R-values in Fig. 8, and (c) a broader, more diffuse neck with increasing R-value in Figs. 6 and 9.

The difficulty of obtaining the plane strain condition with the diffuse neck at high R-values (see Fig. 7) also controls the orientations at which localized necks form (Fig. 9). Given that localized necking occurs along Hill's directions of zero extension, [23] the attainment of near-plane strain

at low R-values (Fig. 7a) results in localized necking nearly normal to the tensile axis (Fig. 9a). In contrast, the strain path within the diffuse neck at high R-values is still near that of simple tension (Fig. 7b) and the corresponding localized neck in Fig. 9c is sharply inclined to the stress axis, lying near the zero extension direction.

A quantitative comparison between the present experimental observations and predictions based on localized theory can be obtained by considering the measured values of the principal limit strain ε_1^* in Fig. 11b with that calculated (see Appendix I) from an extension of the Marciniak-Kuczynski imperfection analysis [24] by Chan, Ghosh and Koss.[25] The model predicts, as is presently observed, that for uniaxial tension increasing the R-value increases the limit strain at the onset of localized necking. Given that $n \simeq 0.05$ and $m \simeq 0.014$, Fig. 11b shows the excellent agreement between the experimental results and predictions from the model using Eq. (1a) of the appendix with a realistically small imperfection of $f = 0.99$ and assuming $\varepsilon_0 = 0$, which implies $\bar{\sigma} = k\,\bar{\varepsilon}^{n}\dot{\bar{\varepsilon}}^{m}$ as a constitutive equation. Furthermore, Chan et al also show that localized necking along Hill's direction of zero extension obeys a critical thickness strain (ε_3^* = material constant) criterion.[25] The magnitude of ε_3^*, which equals approximately 0.08 in the present study, depends on n, m, and the imperfection factor f, but ε_3^* should be independent of R (as is experimentally observed in Fig. 11a). Thus we conclude that for localized necking the increase in the major principal strain ε_1^* with increasing R-value is caused by increasing difficulty of attaining the critical thickness strain ε_3^* at high R and difficult through-thickness slip.

The influence of R-value on the fracture strain ε_{1f} is more complicated. As shown in Fig. 11c, the fracture strain ε_{1f} increases as R increases but at a diminishing rate at large R-values. In addition, the thickness strain at fracture (ε_{3f}) has been found to depend on crystallographic texture and vary

with the R-value. On the other hand, a critical thickness strain criterion [26] has been applied successfully to explain the fracture behavior of textured Ti-6-4 and Ti-5-2.5 sheet deformed under stress states varying from uniaxial to biaxial tension.[21] It thus appears that ε_{3f} is quite sensitive to crystallographic texture but is relatively insensitive to the loading path.

Fractography indicates that fracture is characterized by through-thickness shear exhibiting shallow and small dimples when crystallographic texture allows easy thinning and results in a low R-value (see Fig. 10, R = 0.5). However, at high R-values the fracture strain ε_{1f} is increased and the appearance of the fracture surface indicates a large strain deformation at greater depths from the fracture surface with larger and deeper dimples (see Fig. 10, R = 12). The increase in the depth and the size of dimples as R increases can be explained in terms of the increasing breadth or width of the localized neck with increasing R. This would result in a broader band of intense plastic flow and thus deeper dimples. Experimental evidence appears to support this theory. For Ti-6-4 sheet with R-values ranging from 0.5 to 12, the breadth of the localized neck increases from 0.5mm to 1.3mm. The localized neck for textured sheet with R = 12 has the form of an intense shear band with minimal thinning; the width of the localized neck is less defined and is quite difficult to measure. Visual observation of the shear band while under strain indicates that its size is quite large. In addition, an increase in the volume of material undergoing intense plastic flow as R increases is also evidenced by the increase in the sharpness and a decrease in the profile radius of the diffuse neck with increasing R-value (Fig. 6). Consequently, the thicker band of intense plastic flow associated with the high R-value materials result in larger and deeper dimples and also contributes to an increased fracture strain observed on these materials.

SUMMARY

The influence of crystallographic texture on the tensile deformation and fracture behavior of strongly textured Ti alloy sheet has been studied by uniaxial tensile testing. The study is based on Ti-6Al-4V and Ti-5Al-2.5 Sn sheet with either the basal or the basal-transverse texture. The tensile results indicate that the crystallographic texture strongly affects the yield strength and the ease of through-thickness deformation as measured by the plastic anisotropy parameter, R, which varies from 0.5 to 12 in the material tested. However, work hardening rate n and strain rate hardening exponent m, are relatively insensitive to the differences in slip behavior between the two textures.

Analysis of the tensile behavior at large strains reveals that the strain distribution within the diffuse neck is strongly affected by crystallographic texture through its pronounced influence on the R-value. During deformation the strain state within the diffuse neck deviates from that of uniaxial tension and shifts towards plane strain. This change of strain state results in additional hardening at the center of the diffuse neck, the amount of additional hardening increasing with R. As a result, the diffuse neck becomes broader, and the post-uniform elongation, and the ability to retain the load carrying capacity after maximum load are both enhanced with increasing R-value.

The localized necking may be interpreted in terms a of critical thickness strain criterion; such a criterion is experimentally observed as well as theoretically predicted. Increasing the difficulty of through-thickness deformation thus delays the attainment of the critical thickness strain and increases the limit strain at the onset of localized necking at high R-values. Theoretical calculations of the forming limit strains using an inclined imperfection model are in very good agreement with the experimental results.

The calculations not only predict the enhancement of the limit strain with increasing R-value but also confirm the existence of a critical thickness strain criterion for localized necking in uniaxial tension.

Fractography reveals that fracture of textured Ti-alloy sheet occurs by transgranular void formation and coalescence. The fracture strain increases with increasing R-value with large, deep dimples characterizing the fracture surfaces of sheets with high R-value. This behavior can be interpreted in terms of the increased breadth of intense plastic flow as through-thickness deformation becomes more difficult and $\bar{r}$ increases.

ACKNOWLEDGMENTS

The authors wish to thank Dr. Amit Ghosh for many stimulating discussions and valuable suggestions, Prof. K. Weinmann for technical assistance, Dr. A. Sommer and Del West Associates for supplying Ti-6Al-4V plate with a basal-transverse texture and Mr. R. Boyer of Boeing for the texture determinations.

The program was supported by the Office of Naval Research through Contract No. N00014-76-C-0C37, NR 031-756.

APPENDIX I

In their analysis of localized necking in the negative minor region of the forming limit diagram (i.e., loading paths from uniaxial tension to plane strain), Chan et al [25] extend the Marciniak-Kuczynski (M-K) analysis [24] which associates localized necking of sheet with pre-existing imperfections. The M-K analysis was originally developed for biaxial stretching; the Chan et al analysis extends that analysis to uniaxial tension in which case the imperfections are inclined at an angle ϕ^* (along Hill's direction of zero extension) [23] to the major principal strain axis. For a material which obeys a Swift-type equation $\bar{\sigma} = K(\bar{\varepsilon}_o + \bar{\varepsilon})^n \dot{\bar{\varepsilon}}^m$ and Hill's original yield function for an anisotropic material, [27] Chan et al show that the effective strain with an imperfection ($\bar{\varepsilon}_B$) may be related to that outside the imperfection ($\bar{\varepsilon}_A$) by a numerical solution of the following equation:[25]

$$d\bar{\varepsilon}_A^{\,m}\left[\bar{\varepsilon}_o+\bar{\varepsilon}_A\right]^n \exp[-C\bar{\varepsilon}_A] = f\left[\bar{\varepsilon}_o+\bar{\varepsilon}_B\right]^n \exp[-F\cdot\bar{\varepsilon}_B]d\bar{\varepsilon}_B^{\,m} \qquad (1a)$$

where

$$F = \sqrt{\frac{3}{2}}\sqrt{\frac{1+2R}{(R+2)(R+1)}}\left[1+2(R+1)\ \alpha_2^{\,2}\right]^{-\frac{1}{2}}$$

$$C = \sqrt{\frac{3}{2}}\sqrt{\frac{1+2R}{(R+2)(R+1)}}\left[1+2\rho_2^{\,2}/(R+1)\right]^{-\frac{1}{2}}$$

$$\alpha_2 = \frac{(1-\alpha)\ \sin\phi^*\cos\phi^*}{\cos^2\phi^* + \alpha\ \sin^2\phi^*}\ ;\ \alpha = \frac{\sigma_2}{\sigma_1}$$

$$\rho_2 = \frac{(1-\rho)\ \sin\phi^*\cos\phi^*}{\cos^2\phi^* + \rho\ \sin^2\phi^*}\ ;\quad = \frac{\varepsilon_2}{\varepsilon_1}\ ,$$

and for uniaxial tension:

$$\alpha = \frac{(1+R)\ \rho + R}{1 + R + R\rho} = 0,$$

and

$$\phi^* = 90^\circ - \tan^{-1}\left[\frac{\alpha - \left(\frac{1+R}{R}\right)}{\left(\frac{1+R}{R}\right) - 1}\right]^{\frac{1}{2}}$$

In Eq. 1a, the term f is the imperfection factor, which for sheet containing an imperfection such that it has thicknesses t_A and t_B and strengths K_A and K_B inside and outside the imperfection, is defined as $f = K_B t_B / K_A t_A$.

Given values for n and m, the dependence of the limit strain ε_1^* on R-value can be calculated from Eq. 3 with f being the only adjustable parameter. The model predicts the dependence of localized necking at uniaxial tension on both the work hardening n and strain rate hardening m as well as on the R-value. Of particular interest is that localized necking along Hill's direction of zero extension obeys a critical thickness strain (ε_3^* = material constant) criterion.

References

1. Larson, F. and Zarkades, A., Properties of Texture Titanium Alloys, Report MCIC-74-20, MCIC, Battelle Columbus Laboratories, Columbus, Ohio, 1974.

2. Fitzpatrick, J. M. and Crossley, F. A., Development of Improved Biaxial Strengthening in Titanium Alloy Rocket Motor Cases Through Texture Hardening, Phase 1, AFML-TR-67-302, Dec., 1967.

3. Fredrick, S. F., Many Methods for Production Process for Titanium Sheet with Controlled Textures, AFML-TR-73-265, Nov., 1973.

4. Sommer, A. W. and Creager, M., Research Toward Developing and Understanding of Crystallographic Texture on Mechanical Properties of Titanium Alloys, AFML-TR-76, 222, Jan., 1977.

5. Bowen, A. W., Mat. Sci. and Eng., 1979, vol. 40, p. 31.

6. Tchorzewski, R. M. and Hutchinson, W. B., Met. Trans., 1978, vol. 9A, p. 1113.

7. Bowen, A. W., Acta Met., 1978, vol. 26, p. 1423.

8. Hatch, A. J., Trans. AIME, 1965, vol. 233, p. 44.

9. Lee, D. and Backofen, W. A., Trans. AIME, 1966, vol. 236, p. 1966.

10. Lowden, M.A.W. and Hutchinson, W. B., Met. Trans., 1975, Vol. 6A, p. 441.

11. Fishburn, R. A., Roberts W. T. and Wilson, D. V., Metals Tech., 1976, p. 310-317.

12. Okazaki, K., Kagawa, M. and Conrad, H., Acta Met., 1979, vol. 27, p. 301.

13. K. Okazaki, M. Kagawa and H. Conrad, in Titanium '80, p. 863, TMS-AIME, Warrendale, PA, 1980.

14. P. Kvist in Titanium '80, p. 1121, TMS-AIME, Warrendale, PA, 1980.

15. A. K. Ghosh, J. Eng. Mat'l. Tech. (Trans. AIME), 1977, vol. 99, p. 264.

16. S. S. Hecker, in Formability, Analysis, Modeling, and Experimentation, p. 150, TMS-AIME, New York, 1978.

17. A. N. Bramley and P. B. Mellor, Int. J. Mech. Sci., 1966, vol. 8, p. 101.

18. R.M.S. Horta, W. T. Roberts and D. V. Wilson, Int. J. Mech. Sci., 1970, vol. 12, p. 231.

19. J. Woodthrope and R. Pearce, Sheet Met. Ind., 1969, vol. 46, p. 1061.

20. S. S. Hecker, Sheet Metal Ind., 1975, p. 671.

21. K. S. Chan and D. A. Koss, Technical Report No. 18, Office of Naval Research Contract N00014-76-C-0037, NR 031-756, March, 1982.

22. A. K. Ghosh, Met. Trans., 1974, vol. 4, p. 1607.

23. R. J. Hill, J. Mech. Phys. Solids, 1952, vol. 1, p. 19.

24. Z. Marciniak and K. Kuczynski, Int. J. Mech. Sci., 1967, vol. 9, p. 609.

25. K. S. Chan, A. K. Ghosh and D. A. Koss, to be published.

26. G. LeRoy and J. D. Embury, in Formability, Analysis, Modeling and Experimentation, p. 183, TMS-AIME, New York, 1978.

27. R. Hill, The Mathematical Theory of Plasticity, p. 318, Oxford Univ. Press, Oxford, 1967.